

Supplementary Information

Revealing the effects of cell cycles on cellular uptake of nano-drugs at single particle level

Xinzhe Song[†], Siying Li[†], Jiahui Zhang[†], Hui Wang[†], Yuping Shan^{†, *}

[†]School of Chemistry and Life Science, Advanced Institute of Materials Science, Changchun
University of Technology, Changchun 130012, China.

E-mail: shanyp@ciac.ac.cn

Materials and methods

Materials

The following chemicals and reagents were purchased from Sigma-Aldrich (St. Louis, MO, USA): thymidine, nocodazole, Ro-3306, Camptothecin (CPT), 1-(3-dimethylaminopropyl)-3-ethylcarbodiimide hydrochloride (EDC), and N-hydroxysuccinimide (NHS). Dulbecco's Modified Eagle Medium (DMEM), trypsin Ethylene Diamine Tetraacetic Acid (EDTA), penicillin, and streptomycin were purchased from GIBCO BRL (Gaithersburg, USA). Fetal bovine serum (FBS) was purchased from Hyclone (Buckinghamshire, UK). G7-PAMAM was purchased from the Weihai CY Dendrimer Technology Company. GE11 (YHWYGYTPQNVI) was purchased from Sangon Biotech. The cell cycle and apoptosis analysis Kit was obtained from Beyotime Institute of Biotechnology (Jiangsu, China).

Cell culture

The human non-small cell lung cancer cells (A549) and human embryonic kidney cells (HEK 293T) were obtained from the Shanghai Institute of Biochemistry and Cell Biology. These cells were maintained in DMEM supplemented with 10% FBS, 100 mg/mL penicillin, 100 mg/mL streptomycin, and BIOMYC-3 antibiotic solution. The cells were incubated in a 5% CO₂ atmosphere at 37 °C.

Flow cytometry assays

According to the previous reported method, 35-mm-diameter petri-dish was seeded with ~150,000 cells and incubated for 24 h¹. After synchronizing, cells were centrifuged at 1000 rpm for 5 min, removing supernatant, and cell pellets were resuspended in 1 mL PBS. Then, 1 mL of ice-cold 70% ethanol was added drop-wise to the pellet while vortexing, and cells were maintained at 4 °C for a minimum of 2 h. After centrifuging at 1000 rpm for 5 min at 4 °C, the supernatant was removed and cell pellets were washed twice with PBS before resuspending in 0.2-0.5 mL of propidium iodide (PI)/RNase staining buffer, followed by incubation at room temperature for 30 min in the dark. Stained cells strained through a 35 μm nylon mesh, and loaded onto a NovoCyte Advanteon Dx VBR Flow Cytometer (Agilent Technologies, United States). Annotation of data was performed manually using FlowJo software with a 488 nm laser to determine DNA content.

Synthesis of PAMAM-CPT and PAMAM-CPT-GE11

According to the previous reported method, G7-PAMAM aqueous solution (1 mg/mL) and CPT (2.4 mg) were stirred and mixed overnight with low speed at room temperature². The

precipitate was removed by centrifugation and the supernatant was retained to obtain PAMAM-CPT. Then, GE11, NHS, and EDC were dissolved in and stirred with low speed at room temperature for 3 h to active GE11. After that, the PAMAM-CPT solution was mixed with the activated GE11 aptamer and stirred overnight at room temperature, and the PAMAM-CPT-GE11 was obtained.

The encapsulation efficiency (EE) is used to evaluate how much of the initially introduced drug is successfully encapsulated into the carrier. The calculation formula is:

$$EE(\%) = \frac{W_d}{W_i} \times 100\% \quad (1)$$

Where W_i is the initial dosage of the CPT used. The GE11 Conjugation Efficiency (CE) defined as the percentage of GE11 peptide (targeting ligand) successfully conjugated to the drug delivery system, its calculation method is the same as that of EE in formula (1). The weight (W_d and W_i) is obtained through concentration calculations:

$$W = c \cdot V \cdot M \quad (2)$$

Where V is the volume of the solvent used for dissolving the drug, and M is the molecular weight of the drug. The drug concentration c was calculated by Lambert-Beer's Law:

$$A = \epsilon \cdot c \cdot l \quad (3)$$

In the formula, A represents the absorbance of the measured drug at the corresponding wavelength. The molar absorptivity ϵ of the drug is obtained through ultraviolet spectroscopy measurement, and l is the optical path length, which is usually 1 cm.

AFM tip modification

The AFM tips (MSCT, D-tip with a normal spring constant of 0.03 N/m, Bruker, USA) were cleaned by piranha solution (98% H_2SO_4 : 30% H_2O_2 =7:3, v/v). Then, the AFM tips were incubated by vapor deposition with 50 μ L of 3-aminopropyltriethoxysilane (APTES) and 20 μ L of N, N-diisopropylethylamine, follow the previous reported method³. The silanized AFM tip was combined with a heterobifunctional PEG linker (Acetal-PEG₄₅-NHS, 1 mg/mL) in toluene including 0.5% triethylamine (v/v) solution for 2 h. Immerse the PEG-modified AFM tip in 1% citric acid for 10 min to activate carboxyaldehyde⁴. The AFM tip is then immersed in a mixture of PAMAM-CPT-GE11 and 1 M $NaCNBH_3$ for 2 h. Finally, 10 μ L of 1 M ethanolamine was added to the reaction solution for 15 min to inactivate the unreacted aldehyde group, washed the functionalized AFM tip with PBS for subsequent experiments.

Force tracing measurements

Force tracing measurements were performed using AFM 5500 (Agilent Technologies, United States). The deflection signal of the cantilever was recorded using a 16-bit DA/AD card controlled through LabVIEW software. Data acquisition was conducted under specific parameters to eliminate interference from external sources and surroundings: sampling rate set at 20 kHz and a low-pass filter applied with a cutoff frequency of 100 Hz. The probability of observing force signal is the average value from three independent experimental groups, in each group ~2000 FT (~10 cells) curves were analyzed, and the number of FT curves with the FT signal was divided by 2000. The calculation of the displacement (D) during cellular uptake is shown below⁵ :

$$D = d + h \quad (4)$$

Where d is the bending distance of the AFM tip cantilever, and h is the stretching length of the PEG linker. Due to the force-dependent stretching behavior of PEG, which can be described by the extended worm-like chain (WLC) model⁶, the stretching length of the PEG linker (h) was calculated using the following formula:

$$\frac{FL_p}{k_B T} = \frac{l}{4} \left(1 - \frac{h}{L_0} + \frac{F}{K_0} \right)^{-2} - \frac{l}{4} + \frac{h}{L_0} - \frac{F}{K_0} \quad (5)$$

Where k_B is the Boltzmann constant, T is the absolute temperature, L_p is the persistence length, the enthalpic correction K_0 is 1561 ± 33 pN, and L_0 is the contour length. As previously reported, the unit length of PEG is 4 Å and the terminus is 5 Å; the total estimated contour length for the PEG₄₅ linker is around 194 Å. The bending distance (d) of the AFM tip cantilever was determined by applying Hooke's law:

$$F = k \times d \quad (6)$$

The endocytic force of a single nano-drug and the spring constant of the AFM tip cantilever is denoted as F and k , respectively.

SMFS measurements.

The investigation of the interaction between GE11-EGFR on A549 cells was performed in contact mode. The experiments were conducted at a temperature of 37 °C, which was controlled by a temperature controller 325 (Agilent Technologies, Chandler, AZ). The AFM tips utilized have a normal spring constant of 0.03 N m^{-1} (MSCT, D-tip), and the actual spring constants of the AFM tip cantilevers were determined through the thermal noise method as previously described⁷. The probability of observing the force signal was calculated from more than three independent experiments, for each group, 6000 randomly selected FD curves (~10 cells) were analyzed, and the number of FD curves with force signal is divided by 6000.

Fluorescence imaging

PAMAM-CPT-GE11 (1 mg/mL) was reacted with excess 5-fluorescein (5-FAM, 10 mg/mL)

for 3 h in the dark and then purified using 10 kDa ultrafiltration centrifuge tubes. After growing to the logarithmic growth phase, the cells were treated with cell cycle synchronized inhibitor, PAMAM-CPT-GE11-5-FAM were coincubated with the synchronized cells in serum-free medium for 30 min at 4 °C, and washed three times with PBS. Fluorescence imaging was performed using a Nikon Ti-S fluorescence microscope equipped with a 488 nm He-Ne laser to excite fluorescein. Fluorescence intensity was calculated using ImageJ software.

Nanoindentation experiments and Young's modulus calculation.

The polystyrene microsphere with a diameter of approximate 10 μm was glued onto the AFM tip cantilever (MSCT-010, D, Bruker, USA) with a normal spring constant of 0.06 N/m, and the spring constant was measured as $k = 0.039$ N/m. The results are the average value from three independent experimental groups, for each data set, ~6000 force-distance (FD) curves (~10 cells) were obtained with a speed of 2 $\mu\text{m/s}$ and a scanning range of 2 μm , and the same movement distance (500 nm) of piezoceramics after contact with the cell membrane was kept, and the Young's modulus of the cells (E) was determined by the Hertz model⁸. The equation used to determine Young's modulus is given below:

$$F = \frac{4}{3(1 - \nu^2)} \sqrt{R} \delta^{\frac{3}{2}} \quad (7)$$

Where F is the applied force, E is the Young's modulus, R is the radius of the microsphere, δ is the indentation depth, and ν is the Poisson's ratio. The cells are considered linear, elastic, isotropic, incompressible, and having small strain values, so the Poisson ratio is 0.5.

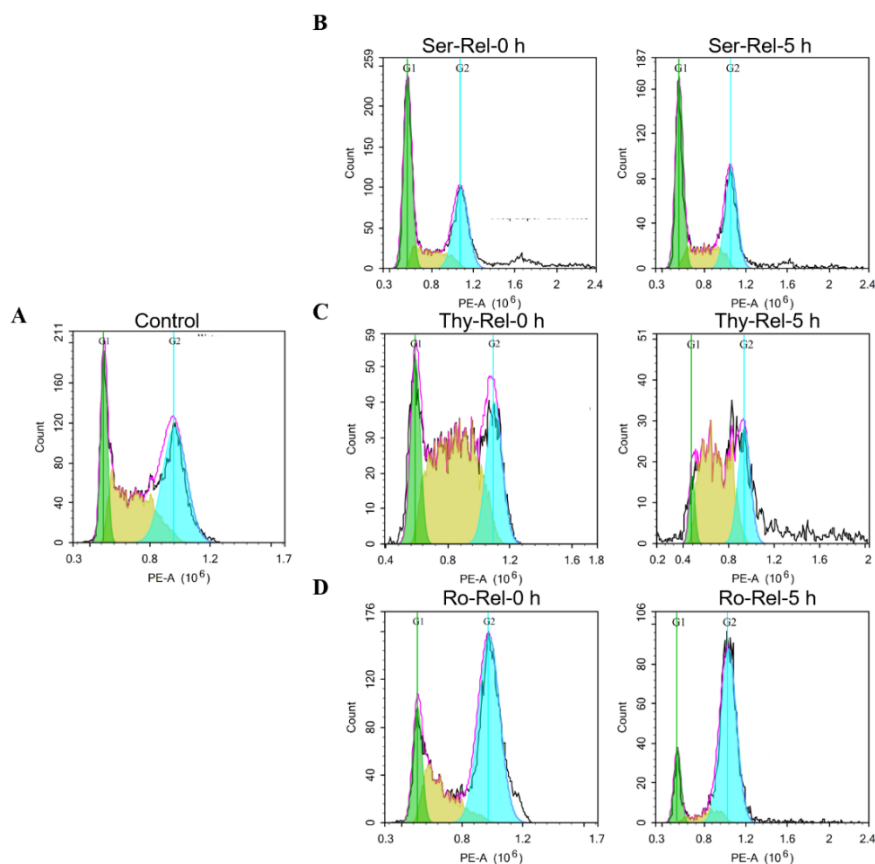


Fig. S1 PI fluorescence profiles of each cell phase on A549 cell. PI fluorescence profiles of A549 cell before treatment (A), after treatment (Rel-0 h), and release (Rel-5 h) from the serum starvation (B), thymidine treated (C), and Ro-3306 treated (D).

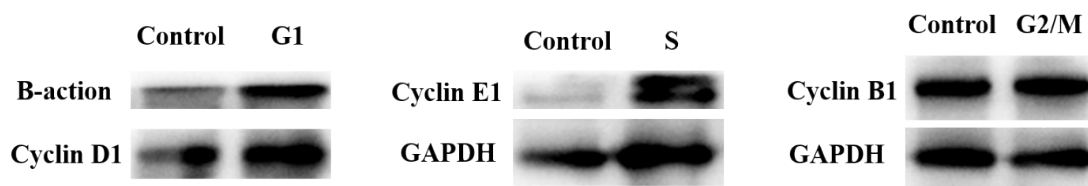


Fig. S2 Western blot analysis of cyclins D1, E1 and B1 expression in A549 cells at G1, S and G2/M phase, respectively. β - actin and GAPDH were used as a loading control to normalize protein expression. Lysates from three biological replicates of each group were loaded.

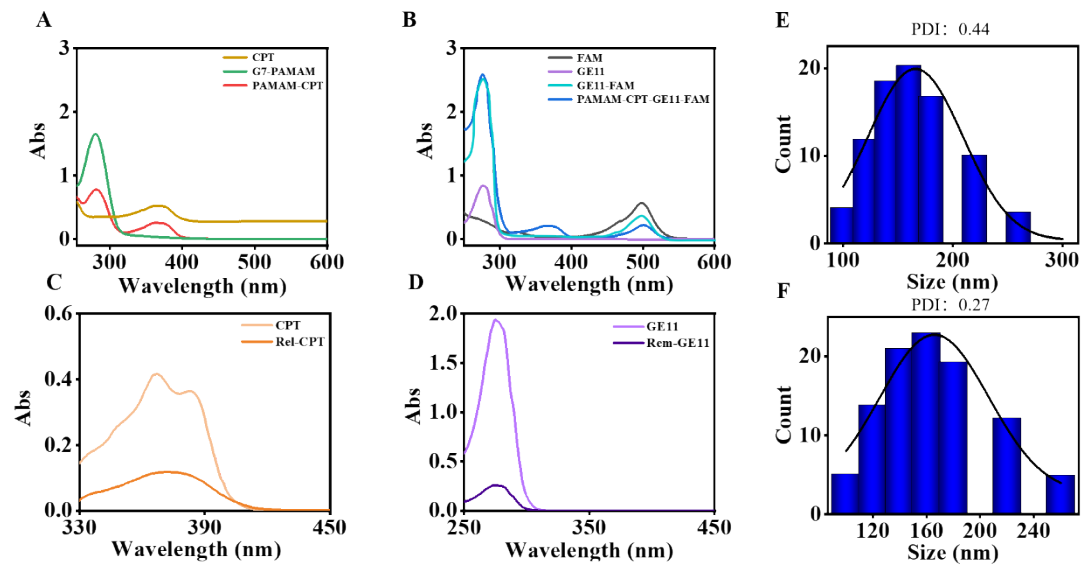


Fig. S3 The characterization of PAMAM-CPT and PAMAM-CPT-GE11. (A) UV-Vis Spectra of G7-PAMAM (orange), CPT (green), and PAMAM-CPT (red). (B) UV-Vis Spectra of FAM (gray), GE11 (purple), GE11-FAM (cyan) and PAMAM-CPT-GE11-FAM (blue). (C) UV-Vis Spectra of initial CPT (iCPT, $\sim 50 \mu\text{M}$) and the released CPT (Rel-CPT) (D) UV-Vis Spectra of initial GE11 (iGE11, $\sim 50 \mu\text{M}$) and remaining GE11 (Rem-GE11). (E) DLS measurement of the particle size distribution of PAMAM-CPT (PDI = 0.44). (F) DLS measurement of the particle size distribution of PAMAM-CPT-GE11 (PDI = 0.27).

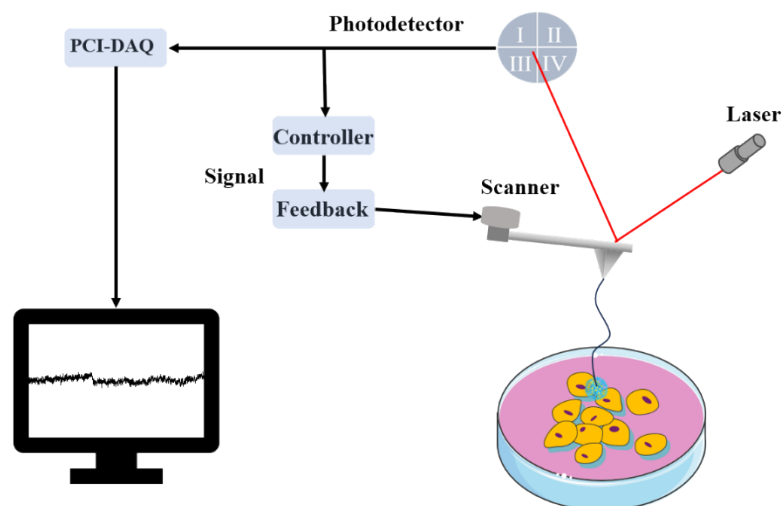


Fig. S4 Schematic diagram of the force tracing technique workflow.

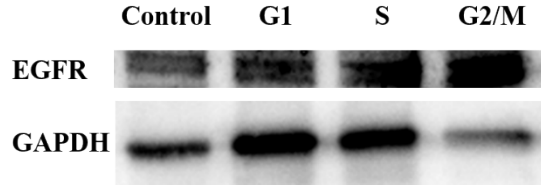


Fig. S5 Western Blot analysis of EGFR expression in A549 cells at different cell cycles. GAPDH was used as a loading control to normalize protein expression. Lysates from three biological replicates of each group were loaded.

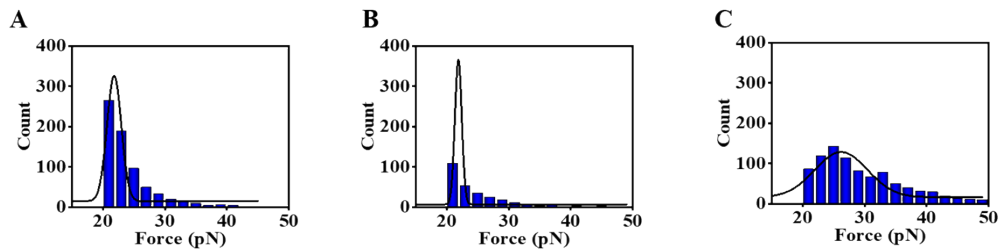


Fig. S6 Histogram distribution of unbinding force for GE11-EGFR in A549 cells in different cycles. (A, B, C) Distribution of the unbinding force for GE11-EGFR on cell in G1, S, and G2/M phase, respectively. ($n \approx 600$)

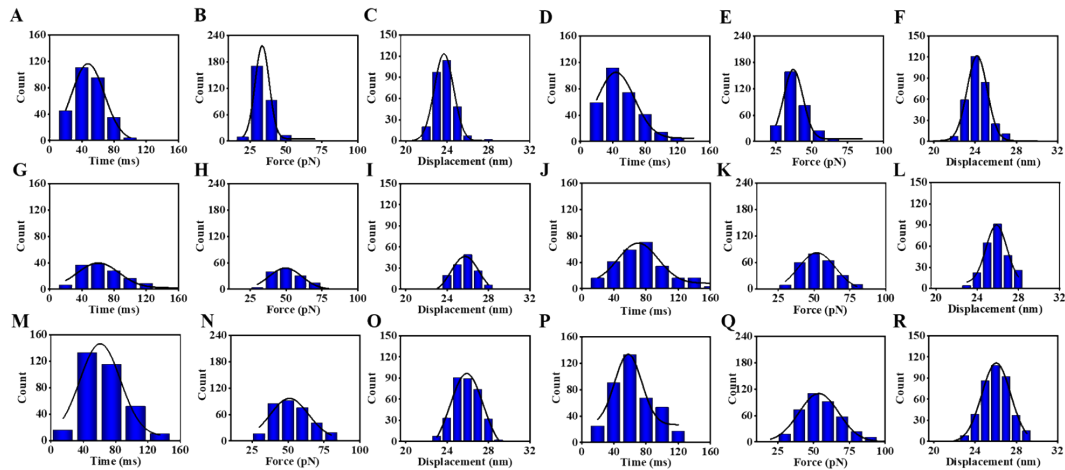


Fig. S7 Histogram of dynamic parameters for nano-drugs entry A549 cell in different cell cycles. (A, G, M) Time distribution histogram of PAMAM-CPT entry cells in G1, S, and G₂/M phases, respectively ($n \approx 250$). (B, H, N) Force distribution histogram of PAMAM-CPT entry cells in G1, S, and G₂/M phases, respectively ($n \approx 250$). (C, I, O) Displacement distribution histogram of PAMAM-CPT entry cells on G1, S, and G₂/M phases, respectively. The solid line is the corresponding Gaussian fit

(n≈250). (D, J, P) Time distribution histogram of PAMAM-CPT-GE11 entry cell in G₁, S, and G₂/M phases (n≈250). (E, K, Q) Force distribution histogram of PAMAM-CPT-GE11 entry cell in G₁, S, and G₂/M phases (n≈250). (F, L, R) Displacement distribution histogram of PAMAM-CPT-GE11 entry cell in G₁, S, and G₂/M phases. The solid line is the corresponding Gaussian fits (n≈250).

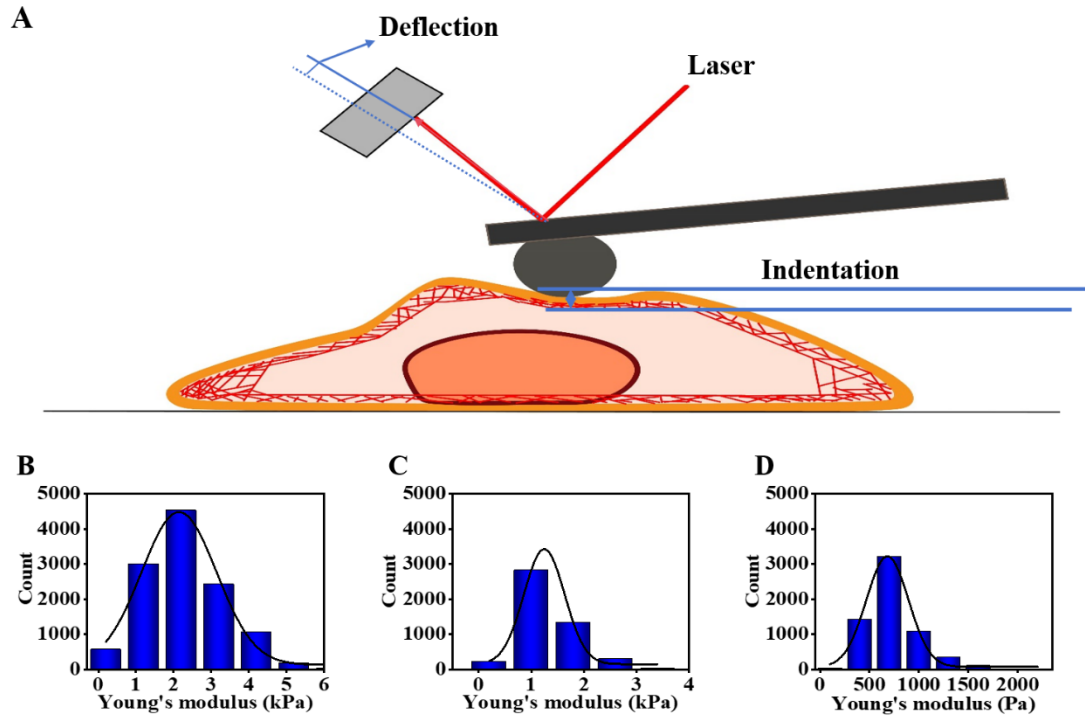


Fig. S8 Nanoindentation measurement of A549 cells based on AFM. (A) Schematic diagram of cytoskeleton deformation during nanoindentation. (B, C, and D) Histogram distribution of the Young's modulus of A549 cells for G₁, S, and G₂/M phase. The solid line is the corresponding Gaussian fit. (n≈6000)

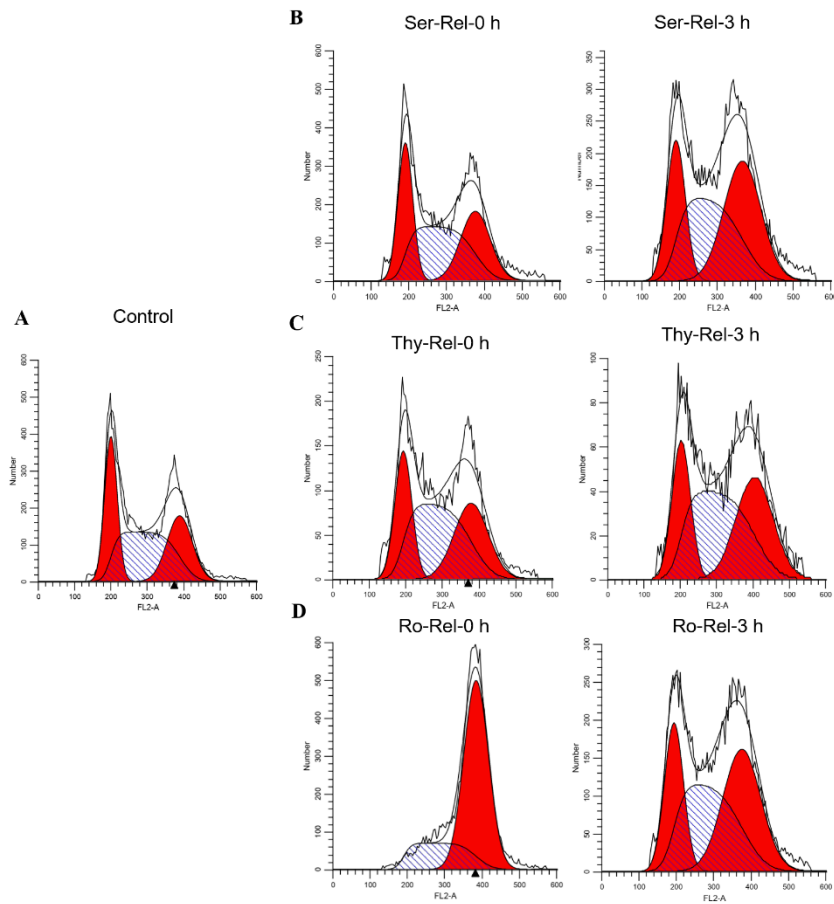


Fig. S9 PI fluorescence profiles of each cell phase on HEK 293T cell. PI fluorescence profiles of A549 cell before treatment (A), after treatment (Rel-0 h), and release (Rel-3 h) from the serum starvation (B), thymidine treated (C), and Ro-3306 treated (D).

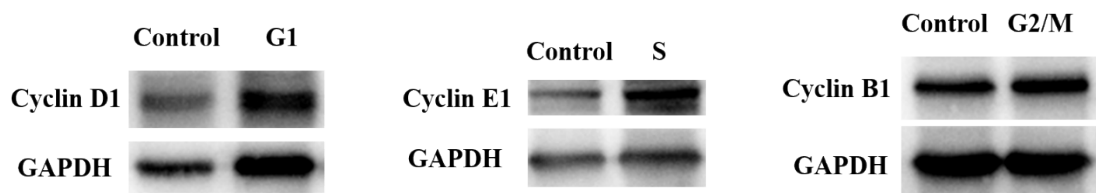


Fig. S10 Western blot analysis of cyclins D1, E1 and B1 expression in HEK 293T cells at G1, S and G2/M phase, respectively. GAPDH was used as a loading control to normalize protein expression. Lysates from three biological replicates of each group were loaded.

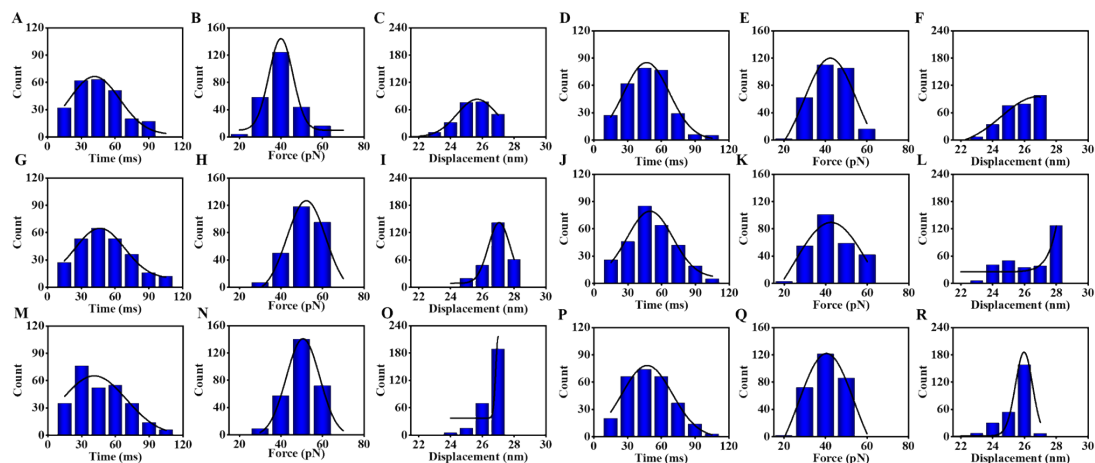


Fig. S11 Histogram of dynamic parameters for nano-drugs entry HEK 293T cell in different cell cycles. (A, G, M) Time distribution histogram of PAMAM-CPT entry cells in G₁, S, and G₂/M phases, respectively ($n \approx 250$). (B, H, N) Force distribution histogram of PAMAM-CPT entry cells in G₁, S, and G₂/M phases, respectively ($n \approx 250$). (C, I, O) Displacement distribution histogram of PAMAM-CPT entry cells on G₁, S, and G₂/M phases, respectively. The solid line is the corresponding Gaussian fit ($n \approx 250$). (D, J, P) Time distribution histogram of PAMAM-CPT-GE11 entry cell in G₁, S, and G₂/M phases ($n \approx 250$). (E, K, Q) Force distribution histogram of PAMAM-CPT-GE11 entry cell in G₁, S, and G₂/M phases ($n \approx 250$). (F, L, R) Displacement distribution histogram of PAMAM-CPT-GE11 entry cell in G₁, S, and G₂/M phases. The solid line is the corresponding Gaussian fits ($n \approx 250$).

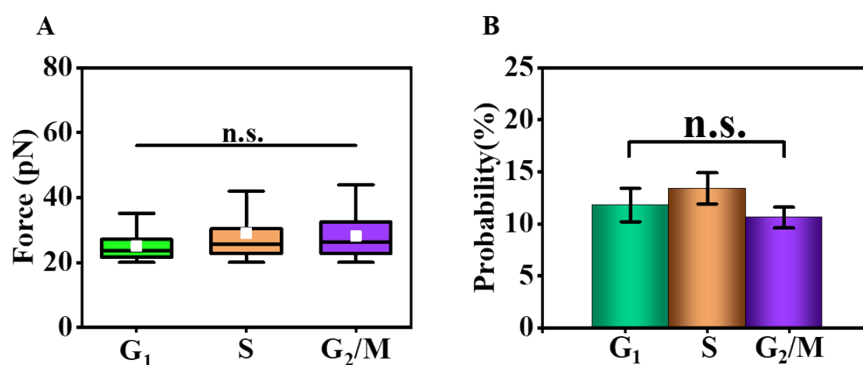


Fig. S12 Detecting the EGFR expression level on the surface of HEK 293T cells in different cell cycles by using SMFS. (A) Distribution of the unbinding force for GE11-EGFR on HEK 293T cells in different cell cycles ($n \approx 350$). (B) The probability of observing the GE11-EGFR unbinding event on HEK 293T cells in different cell cycles. The probability was calculated from more than three independent experiments. For each group,

6000 randomly selected FD curves are analyzed, and the number of FD curves with force signal is divided by 6000.

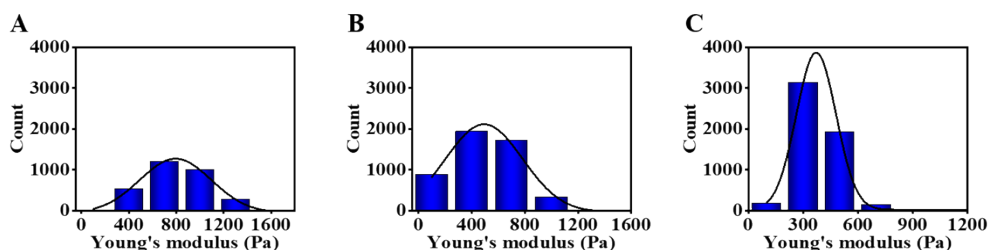


Fig. S13 Histogram distribution of Young's modulus for cells synchronized by nocodazole (A) Histogram of the Young's modulus for cells after release 0 h from nocodazole-treated. (B) Histogram of the Young's modulus of cells after release 1 h from nocodazole-treated. (C) Histogram of the Young's modulus of cells after release 5 h from nocodazole-treated. The solid line is the corresponding Gaussian fit. ($n \approx 6000$)

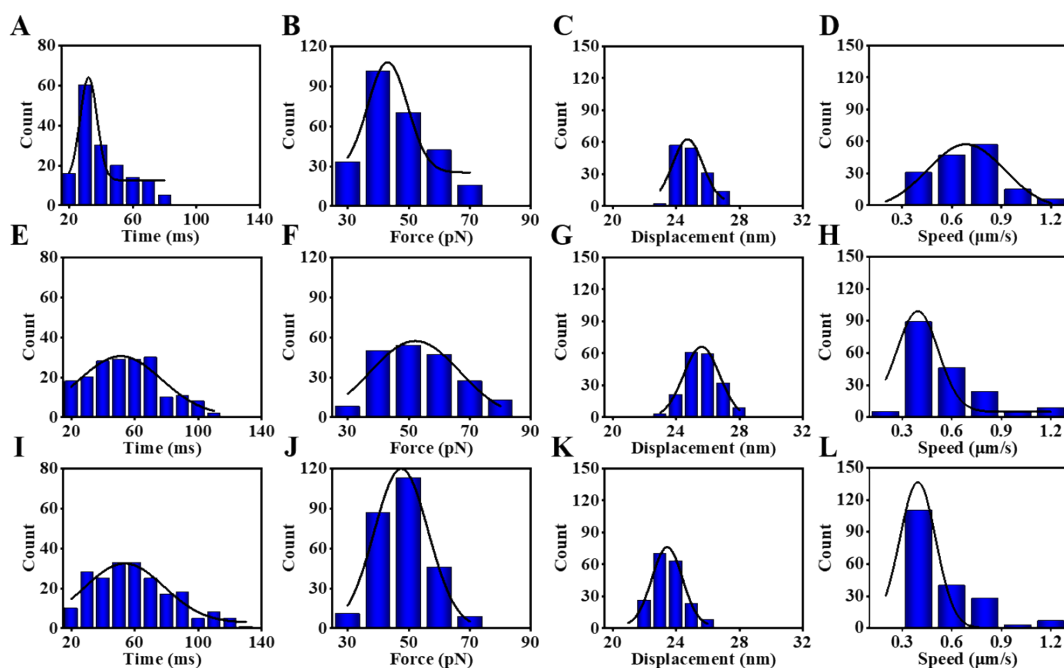


Fig. S14 Histogram of dynamic parameters for PAMAM-CPT entry cell synchronized by nocodazole. (A, E, I) Time distribution histogram of PAMAM-CPT entry cell after release 0 h, 1 h, and 5 h from nocodazole-treated ($n \approx 250$). (B, F, J) Force distribution histogram of PAMAM-CPT entry cell after release 0 h, 1 h, and 5 h from nocodazole-treated ($n \approx 250$). (C, G, K) Displacement distribution histogram of PAMAM-CPT entry cell after release 0 h, 1 h, and 5 h from nocodazole-treated

($n \approx 250$). (D, H, L) Speed distribution histogram of PAMAM-CPT entry cell after release 0 h, 1 h, and 5 h from nocodazole-treated. The solid line is the corresponding Gaussian fit. ($n \approx 250$)

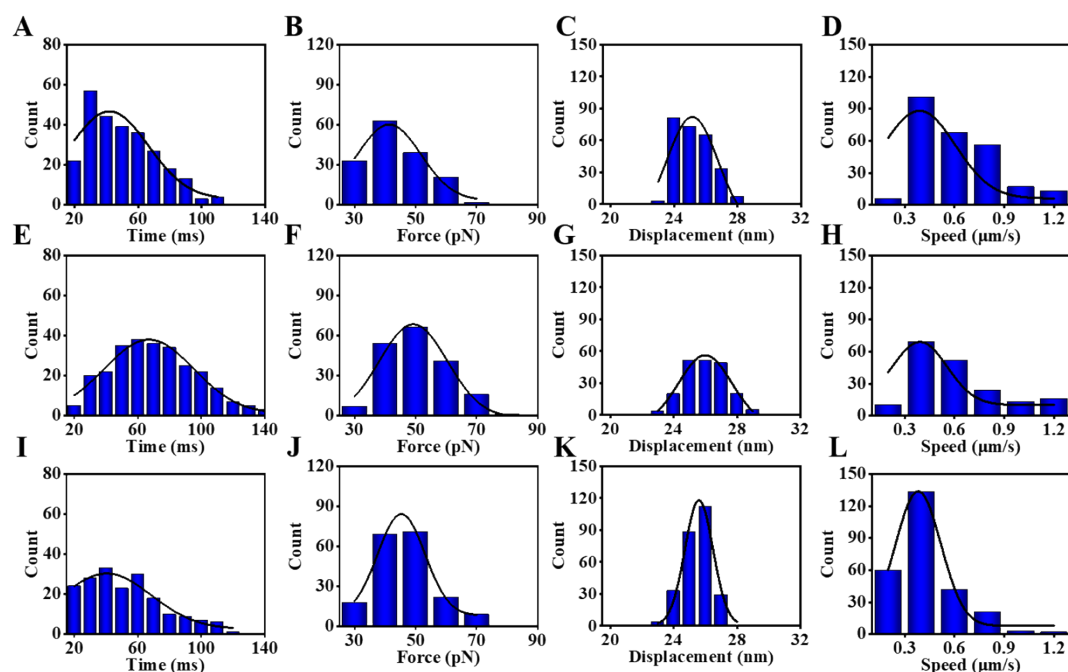


Fig. S15 Histogram of dynamic parameters for PAMAM-CPT-GE11 entry cell synchronized by nocodazole. (A, E, I) Time distribution histogram of PAMAM-CPT-GE11 entry cell after release 0 h, 1 h, and 5 h from nocodazole-treated ($n \approx 250$). (B, F, J) Force distribution histogram of PAMAM-CPT-GE11 entry cell after release 0 h, 1 h, and 5 h from nocodazole-treated ($n \approx 250$). (C, G, K) Displacement distribution histogram of PAMAM-CPT-GE11 entry cell after release 0 h, 1 h, and 5 h from nocodazole-treated ($n \approx 250$). (D, H, L) Speed distribution histogram of PAMAM-CPT-GE11 entry cell after release 0 h, 1 h, and 5 h from nocodazole-treated. The solid line is the corresponding Gaussian fit. ($n \approx 250$)

References

1. S. J. Scott, K. S. Suvarna and P. P. D'Avino, *J. Cell Sci.*, 2020, **133**, jcs247940.
2. M. Shan, H. Wang, S. Li, X. Zhang, G. Yang and Y. Shan, *Mol. Pharmaceutics.*, 2023, **20**, 3234–3240.
3. Y. Liu, Y. Yang, Q. Zhang, D. Lu, S. Li, J. Li, G. Yang and Y. Shan, *J. Mater. Chem. B*, 2021, **9**, 952–957.
4. S. Li, X. Pang, J. Zhao, Q. Zhang and Y. Shan, *NANOSCALE*, 2021, **13**, 17318–17324.

5. Q. S. Li, G. Y. H. Lee, C. N. Ong and C. T. Lim, *Biochem. Biophys. Res. Commun.*, 2008, **374**, 609–613.
6. X. Liao, P. K. Purohit and A. Gopinath, *J. Chem. Phys.* 2020, **153**, 194901.
7. Y.-F. Wang, Q. Zhang, F. Tian, H. Wang, Y. Wang, X. Ma, Q. Huang, M. Cai, Y. Ji, X. Wu, Y. Gan, Y. Yan, K. A. Dawson, S. Guo, J. Zhang, X. Shi, Y. Shan and X.-J. Liang, *ACS Nano*, 2022, **16**, 4059–4071.
8. K. Mendová, M. Otáhal, M. Drab and M. Daniel, *Int. J. Mol. Sci.*, 2024, **25**, 7186.